Discover Applied Sciences

Research

An evaluation of carbon dots derived from *Amaranthus tricolor* (L.) leaves for their physicochemical, photoluminescent, and biomedical properties

Sapam Riches Singh[1] · Santosh Mallikarjun Bhavi[1] · Bothe Thokchom[1] · Megha B. Abbigeri[1] · Akshata Choudhari Padti[1] · Akshata Yadawad[1] · B. P. Harini[2] · Chandramohan Govindasamy[3] · Khalid M. Almutairi[3] · Ramesh Babu Yarajarla[1]

Received: 20 January 2025 / Accepted: 11 April 2025
Published online: 20 May 2025
© The Author(s) 2025 OPEN

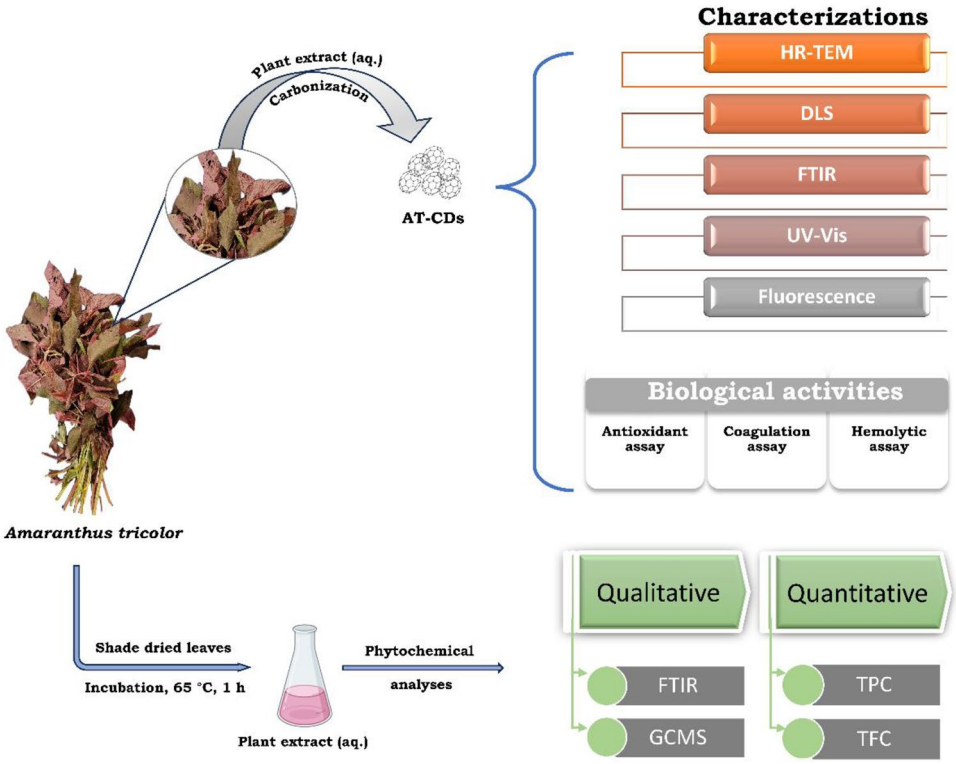
Abstract

This study explores the synthesis, characterization, and bio-functional potential of carbon dots (CDs) derived from *Amaranthus tricolor* (AT-CDs). Phytochemical analysis confirmed the presence of bioactive compounds while quantitative assays revealed a TPC of 157.2 ± 8 mg TAE/g extract and TFC of 457.4 ± 38 mg quercetin/g extract. AT-CDs exhibited a characteristic UV–Vis absorption peak at 317 nm, with fluorescence spectra showing excitation-dependent emission. FTIR analysis identified presence of key functional groups like –OH, –C = O, and –CN, corroborating the bioactive surface chemistry. DLS indicated a Z-average particle size of 214.4 nm, while zeta potential measurements (67.7 mV) confirmed high colloidal stability. TEM analysis revealed a uniform size distribution with a mean particle size of 3.2 ± 0.02 nm. Antioxidant assays demonstrated IC_{50} values of 67.36 µg mL^{-1} for DPPH and 360.65 µg mL^{-1} for H_2O_2 scavenging, reflecting concentration-dependent radical neutralization. Coagulation assays showed a significant prolongation of prothrombin time (55 s) and activated partial thromboplastin time (58 s) at 200 µg mL^{-1}, highlighting anticoagulant potential. These findings suggest that AT-CDs, with their multifunctional properties and bioactivity, are promising candidates for biomedical applications, particularly in oxidative stress management, drug delivery, and haemostasis modulation.

Supplementary Information The online version contains supplementary material available at https://doi.org/10.1007/s42452-025-06936-z.

✉ Ramesh Babu Yarajarla, rameshy@kud.ac.in | [1]Drosophila and Nano-biomedicine Laboratory, Department of Applied Genetics, Karnatak University, Dharwad 580003, India. [2]Department of Zoology and Centre for Applied Genetics, Bangalore University, Bangalore 560056, India. [3]Department of Community Health Sciences, College of Applied Medical Sciences, King Saud University, P. O. Box-10219, 11433 Riyadh, Saudi Arabia.

Graphical abstract



Article highlights

- GCMS revealed methyl 5-methyl-2-thienyl ketone, 2-heptyltetrahydrofuran, squalene, octacosane in plant extract.
- First report of CDs synthesis using *Amaranthus tricolor*.
- AT-CDs act as strong anticoagulation agent.

Keywords Carbon dots · *Amaranthus tricolor* · Green synthesis · Oxidative stress · Coagulation assays

1 Introduction

Nanotechnology is a cross-disciplinary and transformative field that has revolutionized science and technology by offering innovative solutions across various domains, including medicine, agriculture, energy, and environmental remediation [1]. This dynamically evolving paradigm allows the alteration of materials at nanoscale dimensions, bridging the gap between physics, chemistry, biology, and materials science [2, 3]. One of the simplest and most effective method is the green synthesis approach, which has been extensively studied by researchers and proven to be reliable [4]. For instance, green synthesized nanocomposites have shown great potential in water purification, pollutant degradation, and antibacterial activity [5]. Reduced graphene oxide and metal oxide-based nanomaterials offer efficient electrochemical sensing of heavy metals and photocatalytic dye degradation [6]. Carbon-based and doped metal oxide nanocomposites exhibit photocatalytic and antibacterial properties, making them effective against pollutants and microbes [7]. Bimetallic nanocomposites further enhance antimicrobial activity and heavy metal removal, highlighting the significance of biologically synthesized nanomaterials in sustainable environmental solutions [8, 9].

The synthesis of carbon dots, renowned for their excellent fluorescence, biocompatibility, and low toxicity, which makes them ideal for applications in bioimaging, drug delivery, sensors, photocatalysis and ecosystem monitoring, has evolved over the years since its first synthesis in 2004 [10, 11]. Numerous methods are being developed to control their size, morphology, and functionalization [12] [13]. Of these, the technique of using microwave oven has emerged as a versatile, efficient, and eco-friendly approach for producing carbon dots [14]. In this method, microwave irradiation induces localized, rapid and uniform heating, thereby streamlining the conversion of organic precursors into CDs in a matter of minutes [15, 16]. The usage of plant-derived precursors in this process offers an option for sustainable production of CDs, where the use of hazardous chemicals is avoided and bio-functional properties are imparted to the resulting CDs [17–20]. CDs have been synthesized using various green approaches, which shows diverse applications ranging from bioimaging to antioxidant and antibacterial activities, thereby expanding the biomedical scope of plant-based CDs. Some of plant sources used for the synthesis of CDs are listed in Table 1.

Amaranthus tricolor L., commonly known as Joseph's coat or edible amaranth, has proven in several instances its varied importance in medicine [34]. It is a leafy vegetable widely used as a traditional practice in various cultures to treat ailments such as anaemia, gastrointestinal issues, and skin disorders [35–37]. This herbaceous annual plant of the Amaranthaceae family is characterized by its vibrant colours, attributed to its high content of bioactive pigments such as betalains and anthocyanins [38]. *A. tricolor* is a rich source of antioxidants, flavonoids, phenolic acids, vitamins, essential minerals, and are associated with innumerable medicinal benefits, including anti-cancer, antithrombotic, antimicrobial, and anti-inflammatory abilities [39–42]. Due to these several benefits and easy availability, *A. tricolor* serves as a viable precursor for CDs' synthesis.

Thromboembolic disorders, including deep vein thrombosis (DVT), pulmonary embolism, and ischemic stroke, are life-threatening conditions caused by abnormal blood clot formation and impaired vascular function [43]. These disorders are closely linked to oxidative stress, hemolysis, and coagulation imbalances, which contribute to endothelial dysfunction and thrombogenesis [44, 45]. Hemolysis, the breakdown of red blood cells, releases free hemoglobin and iron, leading to oxidative damage that exacerbates inflammation and vascular injury [46]. Oxidative stress, a key factor in thrombus formation, promotes platelet aggregation and disrupts normal blood flow, increasing the risk of embolic events [47]. Moreover, an imbalance in the coagulation cascade can lead to either excessive clotting or bleeding complications, making anticoagulant therapy a critical aspect of thromboembolic disease management [48, 49]. Earlier studies have shown the usage of green synthesized nanoparticles to study their hemocompatibility, antioxidant, antimicrobial and anti-inflammatory properties [50]. CDs synthesized from cassava pulps aid in metal sensing, antioxidants, and mercury detoxification [51]. Traditional Chinese Medicine (the dried pollen of *Typha angustifolia* L., dry rhizome node of *Nelumbo nucifera* Gaerth., dry rhizome node of *Cirsium japonicum* Fisch ex DC., and healthy human hair) derived CDs show hemostatic effects [52]. Investigating the hemolytic, antioxidant, and anticoagulant properties of bioactive compounds could provide potential therapeutic strategies for preventing and managing these disorders, thereby reducing the risk of severe cardiovascular events.

This study underscores the synthesis of CDs derived from *A. tricolor* (AT-CDs) using a microwave-assisted approach and marks the pioneer synthesis CDs from this plant. The plant extract has been tested for the presence of bioactive compounds and the phytochemical content has also been discussed. AT-CDs were thoroughly characterized using various techniques, including UV–visible spectroscopy, fluorescence analysis, FTIR, DLS, and HRTEM, to determine their structural and functional properties. Biological assays including the likes of antioxidant assays and coagulation assays have been performed to give a better understanding of this flora-based CDs. This proof-of-concept study provides the need of the growing relevance of natural products in advanced nanomaterials and their future possibilities of further researches.

2 Methodological approach

2.1 *Leaf extract of Amaranthus tricolor* Linn.

The raw leaves of *Amaranthus tricolor* L., sourced from a local market in Dharwad, Karnataka (15° 27′ 37.17" N, 75° 0′ 51.19" E), were washed with distilled water, microwave-dried (1–2 min), and ground into powder. In a water bath,

Table 1 Comparison of AT-CDs with other plant-derived carbon dots

Source	*Synthesis method*	*Size*	*Applications*	*References*
Spinacia oleracea	Solvent assisted	3 nm	Visual time detection	[21]
Curcuma longa	Hydrothermal assisted	5.13 ± 1.18 nm	Fluorescence probe	[22]
Mixture of plant extracts (*Moringa oleifera and others)*	Solvothermal assisted	15–20 nm	Antioxidant and anti-inflammatory	[23]
Hibiscus rosa-sinensis Linn.	Microwave assisted	12.08 ± 0.52 nm	Wound healing	[24]
Aloe vera	Hydrothermal assisted	4 nm	Photodynamic therapy	[25]
Fresh tea leaves	One pot hydrothermal	2.32 nm	Selective Fe^{3+} ions detection and cellular imaging	[26]
Garlic peel	Microwave assisted	1–9 nm	Pharmaceutical capsules	[27]
Centella asiatica	Microwave assisted	3–6 nm	Antioxidant and anti-inflammatory	[28]
Ficus benghalensis	Hydrothermal Assisted	2.56 nm	Bioimaging	[29]
Lemon and onion	Microwave assisted	4.85 nm	Antibacterial	[30]
Sugarcane bagasse	Hydrothermal carbonisation	27 nm	Antioxidant, reducing and catalytic Activities	[31]
Echinops persicus	Hydrothermal	4–6 nm	Antioxidant	[32]
Water hyacinth	Hydrothermal	1.2–4.9 nm	Photodegradation	[33]
Amaranthus tricolor	Microwave assisted	3.2 ± 0.02 nm	Anticoagulant	Present work

the powdered leaves were used to decoct in distilled water (1:10) for 1 h at 65 °C. The resulting extract underwent filtration via muslin cloth and Whatman grade-I paper, then stored at 15 °C [53].

2.2 Phytochemical profiling

2.2.1 Qualitative analysis of phytochemicals

Phytochemical screening of the extract was conducted to determine the presence of various compounds, as outlined in Table 2, using methods from previous studies [54].

2.2.2 Quantitative analysis of phytochemicals

2.2.2.1 Determination of total phenolic content (TPC) TPC was quantified using the Folin-Ciocalteu method with minor modifications, where, 10% (v/v) Folin-Ciocalteu reagent (2.5 mL) was added to the sample (0.5 mL) and vortexed for 5 min. Potassium iodide (KI) and 7.5% sodium carbonate (0.5 in 2 mL) were introduced, and the mixture was incubated at ambient temperature for 30 min. Absorbance was recorded at 765 nm. A standard calibration curve was prepared using tannic acid solutions (20–100 µg in 2 mL). TPC was expressed in terms of tannic acid equivalents [55].

2.2.2.2 Determination of total flavonoid content (TFC) TFC was determined using a boric acid and oxalic acid-based method. 1 mL of the sample was mixed with 1 mL of 0.1 M boric acid and 1 mL of 0.1 M oxalic acid. The same reagents were used to prepare quercetin standards (20–100 µg mL^{-1}) for the calibration curve. The mixture was incubated at room temperature for 15 min to allow complex formation. The measurement of the absorbance at 230 nm, with ethanol and the acids as a reference blank, was followed by TFC calculation from the calibration curve [56].

Table 2 Phytochemical tests of the presence of bioactive compounds

Phytochemical Tests	*Results*
1. Test for Alkaloids	Absent
• Wagner's test	Absent
• Hager's test	
2. Test for Flavonoids	Absent
• Shinoda test	Present
• Alkaline reagent test	
3. Test for Saponins	Present
• Frothing test	
4. Test for Carbohydrates	Present
• Molisch's test	Present
• Fehling's test	
5. Test for Phenolic Compounds	Present
• Ferric chloride test	Present
• Lead acetate test	
6. Test for Tannins	Present
• Ferric chloride test	Present
• Lead acetate test	
7. Test for Proteins	Absent
• Biuret test	
8. Test for Amino acids	Present
• Ninhydrin test	
9. Test for Terpenoids	Present
• Salkowski test	
10. Test for Glycosides	Present
• Modified Borntrager's test	Present
• Keller Kiliani test	

2.3 Carbon dots synthesis and characterization using the leaves of *A. tricolor*

A microwave-assisted pyrolysis method was used to synthesize AT-CDs from the aqueous extract of the leaves of *A. tricolor*. 15 mL of the plant extract was transferred into a microwave-safe glass container (250 mL borosilicate conical flask) and irradiated at 800 W for 3 to 5 min using a household microwave oven (IFB 20PM-MEC2). The high energy from the microwaves induced rapid heating, leading to the thermal decomposition of organic molecules and the formation of carbon dots. After the reaction, the sample was allowed to cool to room temperature before being centrifuged at 13,000 rpm for 10 min to remove larger particles and impurities. The supernatant containing the synthesized AT-CDs was then filtered through a 0.22 µm syringe filter to further purify the sample. The final product was stored at 4 °C for subsequent analysis and applications.

Comprehensive physico-chemical characterization was performed to determine the optical, structural, and surface properties of AT-CDs. UV–visible spectra were recorded using a JASCO UV–VIS-NIR V-670 spectrophotometer (200–800 nm) with distilled water as the reference. Fluorescence properties were quantitatively assessed with a Hitachi F-7000 fluorescence spectrophotometer. The presence of surface functional groups were able to detect using a Nicolet iS10 FTIR spectrophotometer (400–4000 cm^{-1}). High-resolution transmission electron microscopy (HR-TEM) using a JEOL JEM-2100 Plus (120 kV) revealed the size, shape, and nano structural features of AT-CDs. Zeta potential and size distribution were measured using a Horiba SZ-100 DLS system under optimized conditions of 25 °C, 90° scattering angle, and 0.895 mPa·s viscosity, ensuring colloidal stability.

2.4 Evaluation of Antioxidant Activity of plant extract and AT-CDs

The antioxidant potential of plant extract and AT-CDs was assessed through hydrogen peroxide (H_2O_2) scavenging and DPPH radical scavenging assays. Stock solutions of dried aqueous plant extract, AT-CDs and the standard antioxidant ascorbic acid were prepared in phosphate buffer (1 mg mL^{-1}) and diluted to concentrations ranging from 100 to 600 µg mL^{-1}. Experiments were conducted in triplicate, and the antioxidant activity was expressed as radical scavenging activity (RSA) using the formula:

$$RSA(\%) = \frac{\text{Ab (Control)} - \text{Ab (Test)}}{\text{Ab (Control)}} \times 100$$

where Ab (Control) denotes the absorbance of the control, and Ab (Test) represents the absorbance of the test sample.

2.4.1 Hydrogen peroxide scavenging assay

To prepare the phosphate buffer (pH 7), 13.418 g of sodium phosphate dibasic dihydrate and 2.951 g of sodium phosphate monobasic anhydrous were dissolved in 1000 mL of distilled water. A fresh 40 mM H_2O_2 solution was prepared by diluting 0.408 mL of 30% hydrogen peroxide in 100 mL of phosphate buffer (pH 7.4) and stored in a dark amber flask. For the assay, 1.2 mL of the H_2O_2 solution was mixed with 0.8 mL of plant extract (AT-CDs in case of CDs) solutions at concentrations ranging from 100 to 600 µg mL^{-1}. The reaction mixture was incubated at room temperature for 10 min, and its absorbance was recorded at 230 nm using a blank solution (phosphate buffer without H_2O_2) as the reference [57].

2.4.2 DPPH radical scavenging assay

A 0.2 mM DPPH solution was prepared by dissolving DPPH in methanol. For the assay, 1 mL of the DPPH solution was mixed with 0.5 mL of plant extract (AT-CDs in case of CDs) solutions at concentrations ranging from 20 to 120 µg mL^{-1} and incubated in the dark for 30 min to allow interaction between AT-CDs and DPPH free radicals. After incubation, the absorbance of the samples was measured at 517 nm, corresponding to the characteristic absorption peak of DPPH. The decrease in absorbance at 517 nm was used to calculate the RSA of AT-CDs, demonstrating their free radical scavenging activity [58].

2.5 Coagulation assays

In addition to the antioxidant activity, the potential therapeutic role of AT-CDs was further explored through their effects on blood coagulation, an essential aspect in the management of CVDs. The impact of AT-CDs on clotting times was investigated through prothrombin time (PT) and activated partial thromboplastin time (aPTT) assays using human blood samples. Karnataka Institute for DNA Research, Dharwad provided the ethical approval bearing IEC Ref No. KIDNAR/B[4]/2018-2019.

2.5.1 The prothrombin time (PT)

To perform this test, a thromboplastin reagent substitute (extracted from chicken liver in our case), usually containing tissue factor, is prewarmed, and a calcium chloride ($CaCl_2$) solution is prepared. Blood is collected in a citrate tube that prevents clotting and then centrifuged to separate plasma. During the process, a mixture of 100 µL of plasma and 100 µL of thromboplastin reagent is incubated at 37 °C for 2–3 min. Following this, 100 µL of $CaCl_2$ is added to trigger the clotting process, and the time taken for clot formation is measured.

2.5.2 Activated partial thromboplastin time (aPTT)

The plasma sample is first combined with an activated partial thromboplastin time (aPTT) reagent, which contains a platelet substitute such as phospholipid (either cephalin or lecithin) and a particulate activator, typically kaolin light. These components are essential for mimicking the role of platelets in the coagulation cascade, allowing for the assessment of intrinsic pathway function. The mixture is then incubated at 37 °C for a period of approximately 180 to 240 s, during which time the activation of the coagulation factors takes place. Following this incubation period, calcium chloride ($CaCl_2$) is added to the mixture, which is crucial for the activation of factor X, initiating the final stages of the clotting process. The time required for the formation of a stable, visible clot is then carefully measured and recorded. This clotting time, or the aPTT value, provides a quantitative measure of the plasma's ability to coagulate, reflecting the efficiency and integrity of the intrinsic and common coagulation pathways. This procedure is commonly used to evaluate clotting disorders and monitor anticoagulant therapy.

2.6 Hemolytic assay

Human whole blood was used to perform the hemolytic assay. The sample was collected in a heparin vacutainer and centrifuged for 15 min (1000 × g; 4 °C), ensuring the separation of plasma and the buffy coat. The isolated red blood cells (RBCs) were resuspended after washing thrice with phosphate buffer saline (PBS). A 500 µL aliquot of 30% RBC suspension along with 100 µL of varying concentrations of AT-CDs i.e. 2, 20, 200, 500 and 1000 µg mL^{-1} was incubated for 30 min at 37 °C. The prepared samples underwent centrifugation at 1000 × g post incubation. The supernatant thus obtained was used to measure the absorbance at 620 nm. RBCs treated with 10% DNA lysis buffer and PBS were taken as the positive and negative control respectively. The percentage hemolysis was calculated using the formula:

$$Percentage\ hemolysis = \frac{Absorbance_{test} - Absorbance_{negative\ control}}{Absorbance_{positive\ control} - Absorbance_{negative\ control}} \times 100$$

2.7 Statistical approach

For statistical evaluation, triplicate data were analysed using one-way ANOVA followed by Tukey's HSD test for post-hoc analysis, with all calculations performed using GraphPad Prism 10.1.0. The one-way ANOVA was used to assess overall group differences, while Tukey's test allowed for pairwise comparisons between groups. The significance level was set at $p < 0.05$, and results are presented as mean ± SD. Statistical significance was considered based on the F values obtained, and the data provide a comprehensive view of the variations observed across the experimental groups. The effect sizes, confidence intervals, and precise p-values are included in Table S2.

3 Results and discussion

3.1 Phytochemical profiling: qualitative and quantitative

Phytochemical analysis of *A. tricolor* plant extract confirmed the presence of flavonoids, saponins, carbohydrates, phenolic compounds, tannins, amino acids, terpenoids, and glycosides, highlighting the bioactive nature of the material, which corresponds to the earlier studies (Table 2) [59]. Flavonoids and phenolic compounds are well-known antioxidants, capable of scavenging free radicals and protecting cells from oxidative damage [60, 61]. This suggests

Table 3 Total phenolic, flavonoid contents of aqueous extract of *A. tricolor*

Total phenolic mg TAE/g extract	*Total flavonoids mg Quercetin/g extract*
157.2 ± 8.21	457.4 ± 38

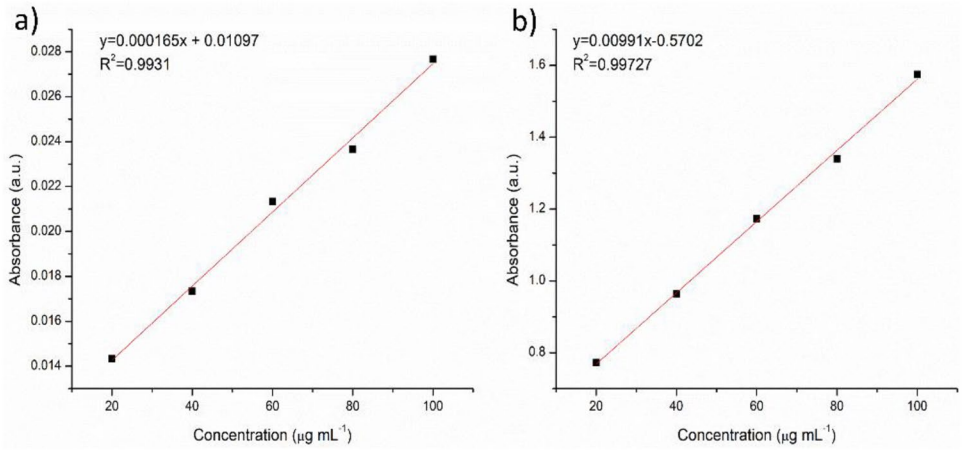


Fig. 1 Calibration curve of **a** quercetin and **b** tannic acid. Each point represents the mean of three experiments

that *A. tricolor* could be highly effective in mitigating oxidative stress-related disorders, making them promising candidates for applications in pharmaceuticals, nutraceuticals, and skincare products [17, 62, 63]. The antioxidant-rich profile may also enhance the biocompatibility and stability of *A. tricolor*, improving their usability in bioimaging, drug delivery, and other biomedical applications. In a study conducted by Tejwan et. al., water-soluble CDs were synthesized from red Korean ginseng root extract via microwave irradiation, which has demonstrated excitation-dependent fluorescence, efficient drug loading and release (12.7%), free radical scavenging activity, low toxicity, and antibacterial effects [64].

Compounds like tannins and terpenoids are associated with antimicrobial, anti-inflammatory, and anticancer properties [65]. Saponins, known for their surfactant-like properties, may contribute to the stabilization of colloidal suspensions, further aiding the dispersion and solubility of the *A. tricolor* in aqueous systems [66]. Glycosides and amino acids provide additional chemical diversity, allowing the functionalization of the carbon dot surface for targeted interactions with biomolecules [67]. The total phenolic and flavonoid contents obtained were 157.2 ± 8 mg TAE/g extract and 457.4 ± 38 mg Quercetin/g extract respectively as mentioned in Table 3. Also, it has been represented graphically in Fig. 1.

The GC–MS analysis of the aqueous extract identified 42 unique compounds from a total of 67 hits (Figure S1 and Table S1), of which the most abundant phytochemicals with medicinal uses being methyl 5-methyl-2-thienyl ketone, 2-heptyltetrahydrofuran, squalene, juvibione, n-octacosane, and n-heptadecanol (Table 4). Squalene possesses cardioprotective, antioxidant, anti-inflammatory, cholesterol control, anticancer and detoxification properties [68]. Octacosane exhibits antibacterial, antitumor, antioxidant and wound-healing potential [69]. Heptadecanol is known for its antimicrobial and anti-inflammatory properties [70]. Although the exact medicinal use of methyl 5-methyl-2-thienyl ketone is unclear, it can serve as a scaffold for drugs with anti-inflammatory, analgesic, and antipyretic properties [71]. 2-Heptyltetrahydrofuran is an organic solvent whose medicinal properties are not fully studied but is considered non-toxic [72]. Juvibione acts as an insect growth and development regulator and can be used as a pesticide [73].

3.2 Physico-chemical characteristics of AT-CDs

The synthesized AT-CDs exhibited a characteristic UV–Vis absorption spectrum with a prominent peak at 317 nm (Fig. 2a), corresponding to an absorbance of approximately 0.5. This distinct absorption peak is indicative of the unique electronic transitions within the AT-CDs, which are influenced by the functional groups and bonding interactions on their surface [74]. The absorption at 317 nm can be attributed to the n-π* electronic transitions. These transitions typically arise from the presence of oxygen-containing functional groups, such as carbonyl (–C = O) or carboxyl (–COOH) groups, commonly found on the surface of carbon dots synthesized from plant-derived precursors. The n-π* transitions occur due to the

Table 4 Major phytochemicals with medicinal uses present in aqueous extract of *A. tricolor* leaves

Compound	Area%	Similarity	Medicinal properties
Methyl 5-methyl-2-thienyl ketone	46.7	68	Scaffold for antioxidant, anti-inflammatory and analgesic drugs
2-Heptyltetrahydrofuran	30.13	86	Green solvent
Squalene	3.43	95	Anti-inflammatory, antioxidant, improves lipid metabolism, reduces LDL, cardioprotective, anticancer
Juvibione	0.83	92	Pesticide
n-Octacosane	0.68	90	Antibacterial, antitumor, antioxidant and wound-healing potential
n-Heptadecanol	0.26	90	Antimicrobial and anti-inflammatory properties

excitation of non-bonding electrons (n) on oxygen atoms to anti-bonding π^* molecular orbitals. This finding aligns with previous studies on carbon dots derived from natural precursors, where oxygen-rich functional groups dominate their surface chemistry [75]. The UV–Vis profile may also include contributions from π–π^* transitions, which are characteristic of conjugated aromatic domains within the carbon core. A previous study highlighted the efficiency of CDs as photocatalysts for degrading organic dyes, with their light absorption and charge separation capabilities arising from the synergistic interplay of graphitic sp^2 domains and amorphous sp^3 regions [76]. The fluorescence spectra of the AT-CDs, observed at excitation wavelengths of 320, 340, 360, and 380 nm, demonstrated excitation-dependent emission intensities (maximum at 465 nm when excited at 360 nm)(Fig. 2b). This behaviour suggests the presence of diverse surface states and emissive traps, characteristic of the heterogeneous structure of the CDs.

The FTIR spectrum of the synthesized AT-CDs and the leaf extract exhibited similar functional groups, with slight variations in peak positions (Fig. 2c). The broad O–H stretching peak appeared at 3301 cm^{-1} in AT-CDs, slightly shifted from 3236 cm^{-1} in the leaf extract. The C–H asymmetric stretching of sp^3-hybridized bonds was observed at 2921 cm^{-1} in AT-CDs, which was absent or less prominent in the leaf extract. The carbonyl (C = O) or aromatic C = C stretching vibration appeared at 1615 cm^{-1} in AT-CDs, closely matching the 1613 cm^{-1} peak in the leaf extract. The –CH bending vibration, likely from methyl or methylene groups, was recorded at 1398 cm^{-1} in AT-CDs, comparable to 1405 cm^{-1} in the leaf extract. The phenolic O–H bending vibration at 1336 cm^{-1} in AT-CDs corresponded to 1322 cm^{-1} in the leaf extract. The C–O stretching vibrations, associated with alcohols, ethers, or esters, appeared at 1057 cm^{-1} in AT-CDs,

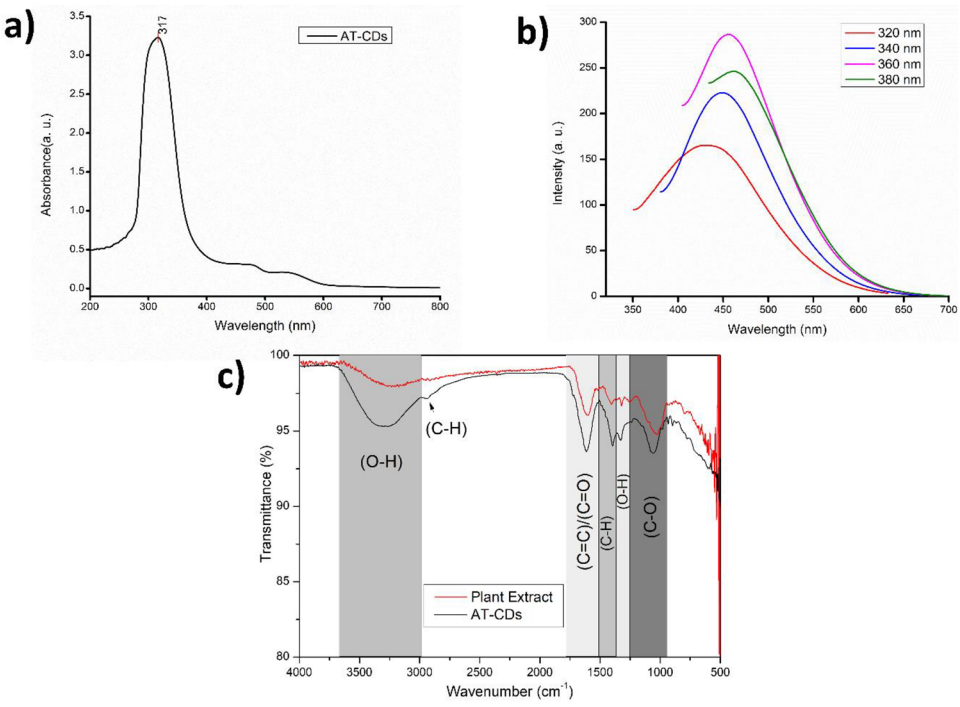


Fig. 2 **a** UV–Visible absorption spectrum of AT-CDs, showing a characteristic peak at 317 nm; **b** fluorescence emission spectra, illustrating the fluorescence intensities; and **c** FTIR spectrum, confirming the presence of functional groups through specific characteristic peaks

slightly shifted from 1047 cm^{-1} in the leaf extract, which also exhibited additional peaks at 1269 cm^{-1} and 1023 cm^{-1}. These similarities suggest the successful incorporation of phytochemicals from the extract into the synthesized AT-CDs while maintaining key functional groups. It can be inferred that the surface of AT-CDs contain hydroxyl (–OH), carboxyl (–COOH), carbonyl (C = O), alkyl (–CH, $–CH_2$, $–CH_3$), phenolic (–OH), ester (–COOR), and ether (–C–O–C) groups. This study corresponds to other earlier study done by Yalshetti et. al., showing various observations of the peaks present [24].

Dynamic Light Scattering (DLS) analysis of the synthesized AT-CDs revealed a Z-average particle size of 214.4 nm with a polydispersity index (PDI) of 0.888, indicating a relatively broad size distribution (Fig. 3b). The high PDI suggests the presence of a heterogeneous population of particles, which may arise from variations in the synthesis process or agglomeration. The zeta potential signified a highly stable colloidal system with a surface charge of 67.7 mV (Fig. 3a). The positive surface charge indicated by the high zeta potential value suggests the presence of cationic functional groups or adsorbed ions, contributing to electrostatic stabilization and preventing aggregation in suspension. These findings align with the functional group analysis and highlight the stability and dispersibility of the AT-CDs in aqueous media. Bhavi et. al., in their study, revealed a particle with moderate stability and reliable particle size, which corresponds with the result obtained [77].

The TEM analysis of AT-CDs at varying magnifications (50 nm, 20 nm and 10 nm) revealed their uniform nanoscale morphology and well-dispersed structure (Fig. 4a, b and c), with a Gaussian distribution curve which indicates a mean particle size of 3.2 ± 0.02 nm (Fig. 4d). This narrow size distribution indicates a high degree of homogeneity in the AT-CDs, which is crucial for their consistent physicochemical properties.

Further structural insights were obtained through high-resolution TEM (HR-TEM), which displayed clear lattice fringes, indicative of the crystalline domains within the AT-CDs. The measured lattice spacing, as determined from the Fast Fourier Transform (FFT) plot inset, was 0.28 nm (Fig. 5), corresponding to the (002) plane of graphitic carbon. This structural feature reflects the hybrid composition of graphitic sp^2 and amorphous sp^3 regions within the AT-CDs. The well-defined d-spacing highlights the graphitic domains that is essential for enhancing charge transport and stability [78]. The strong fluorescence, stability, and surface functional groups of AT-CDs can make them ideal candidates for biosensing, where they can act as fluorescence probes for detecting biomolecules, metal ions, or pH variations. Moreover, their redox-active functional groups and high zeta potential facilitate interactions with various analytes, enabling environmental monitoring applications such as detecting pollutants, heavy metals, or reactive oxygen species (ROS) [79]. In bioimaging, their tunable emission and biocompatibility (discussed in later sections) should allow for cellular tracking and diagnostic imaging without significant cytotoxicity [12].

3.3 Antioxidant activity of AT-CDs

The antioxidant activities of AT-CDs, plant extract, and vitamin C (standard) were evaluated using DPPH and H_2O_2 scavenging assays (Fig. 6). The H_2O_2 scavenging assay revealed a concentration-dependent increase in activity, with vitamin C (90.82%) showing the highest scavenging at 500 µg mL^{-1}, followed by AT-CDs (77.17%) and the plant extract (69.58%). The IC_{50} values of vitamin C (282.24 µg mL^{-1}), AT-CDs (334.75 µg mL^{-1}), and the plant extract (372.54 µg mL^{-1}) indicate that AT-CDs exhibit moderate peroxide-neutralizing capacity, likely due to electron transfer mechanisms facilitating H_2O_2 reduction. The H_2O_2 scavenging capability of AT-CDs were lesser than those of CDs synthesized using *Centella asiatica* [28].

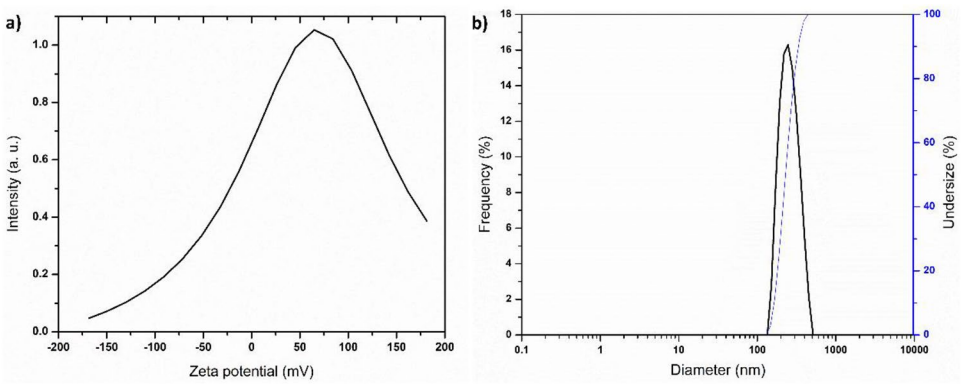


Fig. 3 Dynamic light scattering (DLS) analysis, showing **a** zeta potential measurement, and **b** the particle size distribution and polydispersity index, indicating the surface charge stability of the carbon dots

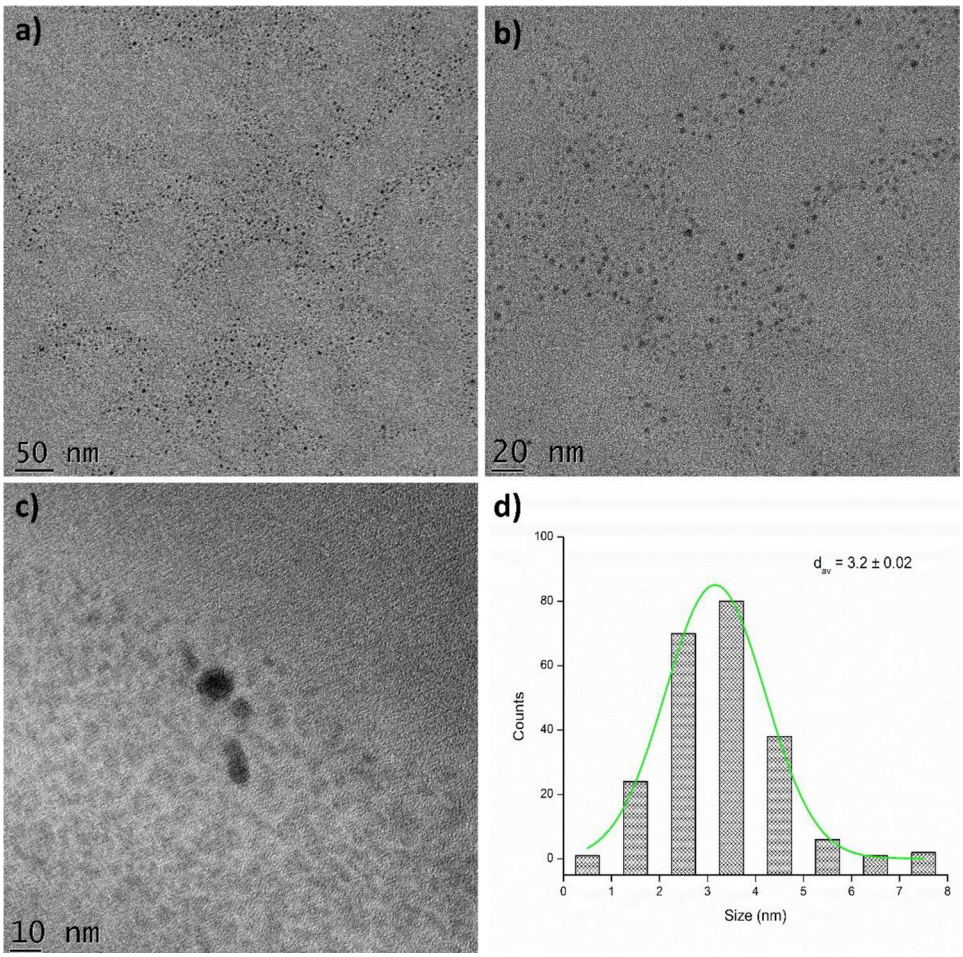


Fig. 4 TEM images of AT-CDs captured at different magnifications: **a** 50 nm, **b** 20 nm, **c** 10 nm; and **d** Gaussian distribution curve illustrating the size distribution of the AT-CDs

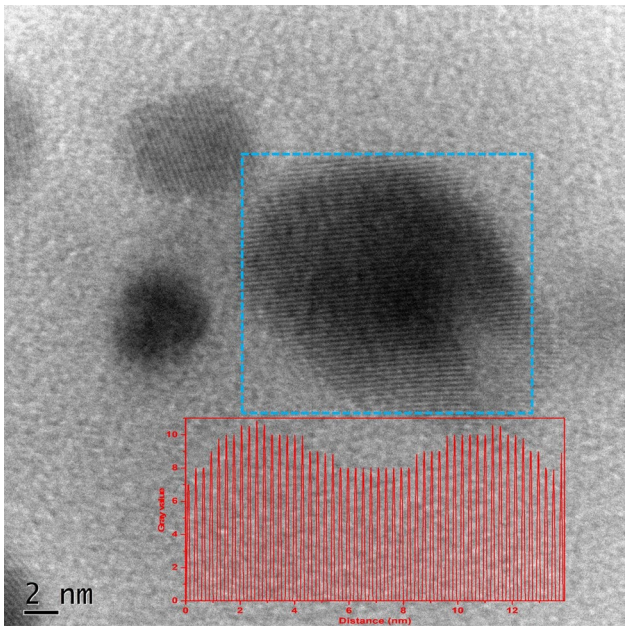


Fig. 5 HR-TEM image at 2 nm showing fast Fourier transfer (FFT) plot profile (red) of the lattice spacing of the particle with the inset (blue boundary)

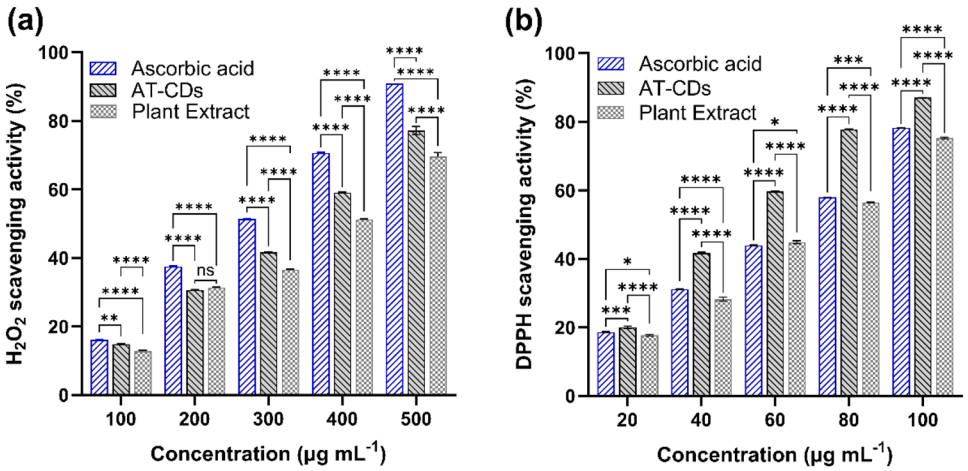


Fig. 6 Antioxidant properties of AT-CDs, aqueous plant extract and vitamin C (standard) using **a** H_2O_2 and **b** DPPH scavenging activities. Results are expressed as mean ± SD (**$p < 0.01$, ****$p < 0.0001$, $n = 3$)

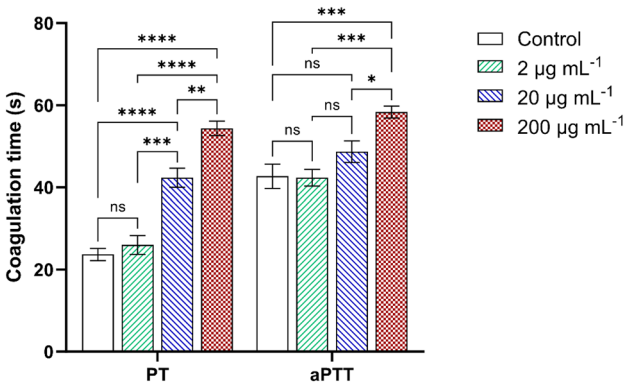


Fig. 7 Coagulation properties investigated with the help of PT and aPTT tests. Results are expressed as mean ± SD ($^{ns}p > 0.05$, *$p < 0.05$, **$p < 0.01$, ***$p < 0.001$, ****$p < 0.0001$, $n = 3$)

In the DPPH assay, a similar trend was observed, where radical scavenging increased with concentration. AT-CDs (87.05%) showed the highest activity at 100 µg mL^{-1}, surpassing vitamin C (78.24%) and the plant extract (75.25%). The lower IC_{50} value of AT-CDs (51.46 µg mL^{-1}) compared to vitamin C (65.49 µg mL^{-1}) and the plant extract (67.66 µg mL^{-1}) suggests a stronger ability to donate electrons or hydrogen atoms, effectively neutralizing free radicals. Moreover, when compared to *Centella asiatica* derived CDs that exhibit an IC_{50} of 165.28 g mL^{-1}, AT-CDs scavenged DPPH more efficiently [28].

These findings highlight the superior DPPH scavenging efficiency of AT-CDs, while their H_2O_2 scavenging ability remains comparable to standard antioxidants. The antioxidant capabilities of *A. tricolor* aqueous extract can be ascribed to the presence of antioxidant bioactive compounds such as squalene, octacosane and heptadecanol as found through GC–MS. In the case of AT-CDs, the hydroxyl, carboxyl, and phenolic groups can donate hydrogen atoms to neutralize free radicals, while the carbonyl and ether groups can participate in electron donation to stabilize reactive oxygen species [80]. This process may give rise to radicals on the CDs, which can be stabilized by alterations in surface chemical bonding or by electron delocalization in the aromatic domain of the CDs' core [81].

3.4 Coagulation assays

The coagulation assays, specifically prothrombin time (PT) and activated partial thromboplastin time (aPTT), were performed to assess the effects of various sample concentrations on blood clotting (Fig. 7). The control group, with a PT of 24 s and aPTT of 44 s, provided baseline coagulation times, reflecting normal clotting function. Upon treatment with 200 µg mL^{-1} of the test sample, a significant prolongation of both PT (55 s) and aPTT (58 s) was observed, indicating a notable effect on coagulation pathways. This suggests that the higher concentration of the sample interferes with either the extrinsic or intrinsic coagulation mechanisms, potentially through antioxidant modulation or other

biochemical interactions. As the sample concentration decreased, the PT and aPTT values gradually returned to control-like levels, though still slightly prolonged, with 20 µg mL^{-1} and 2 µg mL^{-1} concentrations showing PT values of 43 s and 26 s, respectively, and aPTT values of 49 s and 42 s. Antioxidants are known to influence the coagulation cascade by interacting with oxidative stress pathways that can affect clotting factor activation [82]. These findings reflect the dose-dependent effects of the sample on coagulation, which may be attributed to its bioactive compounds, potentially derived from its antioxidant properties [83].

Compared to previous studies on nanomaterials, our findings align with reports that nanoparticles can interact with coagulation proteins and modulate clotting pathways. In a study, green synthesized galbanic acid silver nanoparticles (GA-AgNPs) did not significantly alter PT and aPTT values, maintaining them within normal physiological levels (PT: 9.4–12.5 s; aPTT: 25.1–36.5 s), which suggests their safety for clinical applications [84]. Similarly, Isoimperatorin-mediated green-synthesized silver nanoparticles at concentrations ranging from 50 to 400 µg mL^{-1} exhibited no change in PT and aPTT, that again confirms the minimal impact in the coagulation pathways [85]. However, in an earlier study, *Achillea wilhelmsii* C. Koch synthesized silver nanoparticles at concentrations (0.5–1 mg mL^{-1}) significantly prolonged clotting time up to 3 min, which is an indication of its strong anticoagulant properties [86].

3.5 Hemolysis assay

The hemolytic assay revealed minimal RBC lysis across all tested concentrations, indicating the biocompatibility of the samples (Fig. 8). Hemolysis remained low, with 0.14% at 2 µg mL^{-1}, gradually increasing to 0.23% at 1000 µg mL^{-1}, demonstrating a concentration-dependent effect. Even at the highest concentration, the hemolysis percentage remained well below the 5% safety threshold, suggesting that the samples pose no significant risk of cytotoxicity to RBCs. This low hemolytic activity supports their potential for biomedical applications, particularly in drug delivery and anticoagulation therapies, where hemocompatibility is essential. AT-CDs exhibit better biocompatibility when compared to other plant based CDs such as those synthesized using *Citrus limetta* peels and *Hibiscus rosa-sinensis* leaves [24, 87].

4 Conclusion

This study highlights the potential of AT-CDs as a biocompatible and effective anticoagulant agent with non-hemolytic properties, making them suitable for biomedical applications. Their strong antioxidant activity, surface functional groups, and high zeta potential suggest a role in preventing oxidative stress-related thrombotic disorders. The findings indicate their potential use in therapeutic formulations or as anticoagulant coatings for medical devices. However, computational studies, along with in vivo models, are essential to assess their safety, pharmacokinetics,

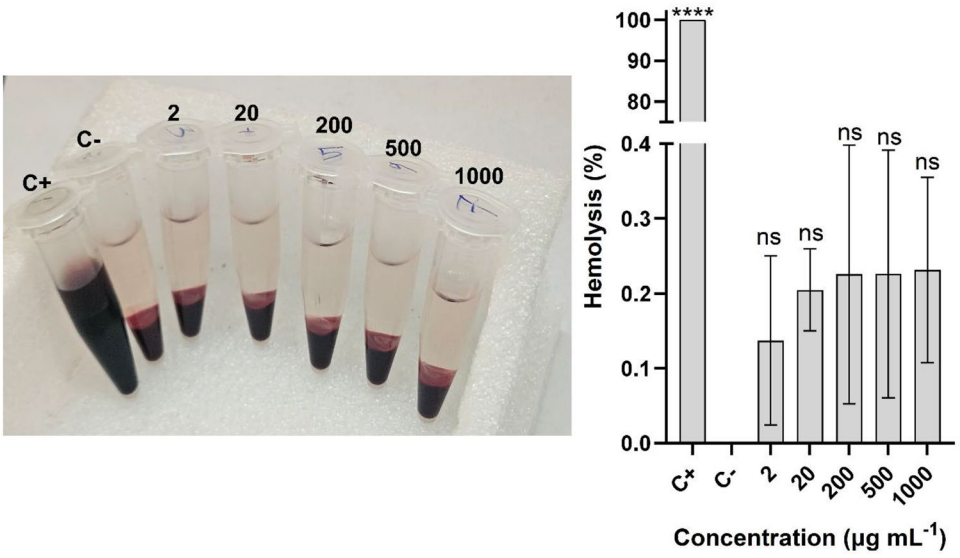


Fig. 8 Hemolytic assay showing centrifuged RBC samples treated with different AT-CDs concentrations. C+, C−, 2, 20, 200, 500, 1000 correspond to positive control, negative control, and those treated with 2, 20, 200, 500 and 1000 µg mL^{-1} AT-CDs respectively. The graph quantifies hemolysis, revealing minimal RBC lysis and high hemocompatibility. $^{ns}p > 0.05$, $^{****}p < 0.0001$, $n = 3$, when compared with negative control

efficacy, long-term stability, potential interactions within complex biological systems and clinical potential. Future research should explore their mechanism of action at the molecular level, optimize their formulation for clinical use, and assess their broader biomedical applications, including targeted drug delivery and real-time blood monitoring. Scalable synthesis, gene regulation studies, and regulatory assessments will ensure their viability for pharmaceutical and nutraceutical use, unlocking their full biomedical potential.

Acknowledgements The author wishes to express sincere gratitude Researchers Supporting Project number (RSPD2025R712), King Saud University, Riyadh, Saudi Arabia for financial assistance. We gratefully acknowledge the invaluable support of the Sophisticated Test & Instrumentation Centre, Cochin University of Science and Technology, for their assistance with TEM analysis. We also extend our appreciation to the Department of Applied Genetics, Karnatak University, Dharwad. Special thanks to the Sophisticated Analytical Instrument Facility (SAIF), Dharwad, Karnatak University, and the DST PURSE Phase-II Program and University Scientific Instrumentation Centre (USIC) of Karnatak University, Dharwad, for their assistance with various analytical techniques. We would like to appreciate Karnataka Institute for DNA Research (KIDNAR) for giving the ethical approval for this study.

Author contributions S.R.S. led the conceptualization, methodology, formal analysis, investigation, data curation, original draft preparation, and visualization. S.M.B., B.T., and M.B.A. collectively contributed to formal analysis, software development, and data curation. A.Y. provided essential support in methodology development, while C.G. and K.M.A. were responsible for funding acquisition. R.B.Y. played a central role in validation, project administration, supervision, and resource allocation. A. C. P. and B. P. H. were involved in reviewing and editing. All authors actively participated in reviewing and editing the manuscript to enhance its clarity and precision.

Funding This research was supported by Researchers Supporting Project number (RSPD2025R712) Department of Community Health Sciences, College of Applied Medical Sciences, King Saud University.

Availability of data and materials The data that support the findings of this study are available from the corresponding author upon reasonable request.

Declarations

Ethics approval and consent to participate Institutional ethical approval was granted by Karnataka Institute for DNA Research (KIDNAR), Dharwad (IEC Ref No. KIDNAR/B[4]/2018–2019). Verbal consent was obtained from all individual participants included in the study while the requirement for written consent was waived by the institutional review board. All procedures performed in studies involving human participants were in accordance with the Helsinki declaration as revised in 2013 and its later amendments. The plant materials were cultivated and collected in compliance to national guidelines and legislation. Verbal informed consent was obtained prior to the interview. The requirement of written consent was waived by the Karnataka Institute for DNA Research (KIDNAR), Dharwad, Karnataka, India.

Consent for publication The authors affirm that human research participants provided informed consent for publication for any data. The results/data/figures in this submission have not been previously published, or are under consideration for publication elsewhere.

Competing interests The authors declare no competing interests.

Open Access This article is licensed under a Creative Commons Attribution 4.0 International License, which permits use, sharing, adaptation, distribution and reproduction in any medium or format, as long as you give appropriate credit to the original author(s) and the source, provide a link to the Creative Commons licence, and indicate if changes were made. The images or other third party material in this article are included in the article's Creative Commons licence, unless indicated otherwise in a credit line to the material. If material is not included in the article's Creative Commons licence and your intended use is not permitted by statutory regulation or exceeds the permitted use, you will need to obtain permission directly from the copyright holder. To view a copy of this licence, visit http://creativecommons.org/licenses/by/4.0/.

References

1. Abbigeri MB, et al. Potential in vitro antibacterial and anticancer properties of biosynthesized multifunctional silver nanoparticles using *Martynia annua* L. leaf extract. Nano Struct Nano Objects. 2024. https://doi.org/10.1016/j.nanoso.2024.101320.
2. Nandipati M, et al. Bridging nanomanufacturing and artificial intelligence—a comprehensive review. Materials. 2024. https://doi.org/10.3390/ma17071621.
3. Singh NB, et al. Nano revolution: exploring the frontiers of nanomaterials in science, technology, and society. Nano Struct Nano Objects. 2024. https://doi.org/10.1016/j.nanoso.2024.101299.
4. Bhavi SM, et al. Green synthesis, characterization, antidiabetic, antioxidant and antibacterial applications of silver nanoparticles from *Syzygium caryophyllatum* (L.) alston leaves. Process Biochem. 2024. https://doi.org/10.1016/j.procbio.2024.06.017.
5. Liang Y, et al. Bioengineering of green rGO/Fe3O4 nanocomposites for rapid cadmium sensing and dye decomposition. Ceram Int. 2025. https://doi.org/10.1016/j.ceramint.2024.11.501.
6. Liang Y, et al. Green synthesis of reduced graphene oxide nanosheets: an efficient material for electrochemical sensor and photocatalytic agent. Microchem J. 2025. https://doi.org/10.1016/j.microc.2025.112799.

7. Zhan Q, et al. Green engineered Mo-CeO_2@C nanocomposites for visible light-assisted dye decomposition and microbial apoptosis. Ceram Int. 2024. https://doi.org/10.1016/j.ceramint.2024.09.086.
8. Huang X, et al. Biological synthesis of bimetallic hybrid nanocomposite: a remarkable photocatalyst, adsorption/desorption and antimicrobial agent. Appl Surf Sci Adv. 2023. https://doi.org/10.1016/j.apsadv.2023.100446.
9. Hasan M, et al. A comparative study on green synthesis and characterization of Mn doped ZnO nanocomposite for antibacterial and photocatalytic applications. Sci Rep. 2024. https://doi.org/10.1038/s41598-024-58393-0.
10. Mankoti M, et al. Exploring the potential of eco-friendly carbon dots in monitoring and remediation of environmental pollutants. Environ Sci Pollut Res. 2024. https://doi.org/10.1007/s11356-024-33448-x.
11. Ge G, et al. Carbon dots: synthesis, properties and biomedical applications. J Mater Chem B. 2021. https://doi.org/10.1039/D1TB01077H.
12. Qureshi ZA, et al. Carbon dots as versatile nanomaterials in sensing and imaging: efficiency and beyond. Heliyon. 2024. https://doi.org/10.1016/j.heliyon.2024.e31634.
13. Xu J, et al. Advancements in the synthesis of carbon dots and their application in biomedicine. J Photochem Photobiol, B. 2024. https://doi.org/10.1016/j.jphotobiol.2024.112920.
14. Li Z, et al. Advanced mechanisms and applications of microwave-assisted synthesis of carbon-based materials: a brief review. Nanoscale Adv. 2025. https://doi.org/10.1039/D4NA00701H.
15. Nazar M, et al. Microwave synthesis of carbon quantum dots from arabica coffee ground for fluorescence detection of Fe3+, Pb2+, and Cr3+. ACS Omega. 2024. https://doi.org/10.1021/acsomega.4c02254.
16. Soledad-Flores O, et al. Rapid synthesis of non-toxic, water-stable carbon dots using microwave irradiation. Micro. 2024. https://doi.org/10.3390/micro4040040.
17. Ngoc LTN, et al. Plant extract-derived carbon dots as cosmetic ingredients. Nanomaterials. 2023. https://doi.org/10.3390/nano13192654.
18. Khan AU, et al. Advancements in the green synthesis of carbon dots for sustainable development. Sustain Mater Technol. 2024. https://doi.org/10.1016/j.susmat.2024.e01004.
19. Jose J, et al. A short review on natural precursors-plant-based fluorescent carbon dots for the targeted detection of metal ions. Sustain Chem Environ. 2024. https://doi.org/10.1016/j.scenv.2024.100114.
20. S., A.K. et al. A review on plant derived carbon quantum dots for bio-imaging. *Materials Advances*. (2023). https://doi.org/10.1039/D3MA00254C.
21. Xu X, et al. Red-emissive carbon dots from spinach: characterization and application in visual detection of time. J Lumin. 2020. https://doi.org/10.1016/j.jlumin.2020.117534.
22. Vadia FY, et al. Development of simple fluorescence analytical strategy for the detection of triazophos using greenish-yellow emissive carbon dots derived from curcuma longa. J Fluoresc. 2023. https://doi.org/10.1007/s10895-023-03548-x.
23. Kota S, et al. Heteroatom-doped carbon dots from medicinal plants as novel biomaterials for as-use biomedical applications in comparison with synthetic drug, zaltoprofen. Sci Rep. 2024. https://doi.org/10.1038/s41598-024-63700-w.
24. Yalshetti S, et al. Microwave-assisted synthesis, characterization and in vitro biomedical applications of Hibiscus rosa-sinensis Linn.-mediated carbon quantum dots. Sci Rep. 2024. https://doi.org/10.1038/s41598-024-60726-y.
25. Karimi M, et al. Development of a novel nanoformulation based on aloe vera-derived carbon quantum dot and chromium-doped alumina nanoparticle (Al_2O_3:Cr@Cdot NPs): evaluating the anticancer and antimicrobial activities of nanoparticles in photodynamic therapy. Cancer Nanotechnol. 2024. https://doi.org/10.1186/s12645-024-00260-8.
26. Ge G, et al. Green synthesis of nitrogen-doped carbon dots from fresh tea leaves for selective Fe3+ ions detection and cellular imaging. Nanomater. 2022. https://doi.org/10.3390/nano12060986.
27. Saber YA, et al. Garlic peel-based carbon quantum dots as a sustainable alternative for the sensitive and green spectrofluorometric quantification of molnupiravir in pharmaceutical capsules. Heliyon. 2024. https://doi.org/10.1016/j.heliyon.2024.e40661.
28. Thokchom B, et al. Green synthesis, characterization and biomedical applications of Centella asiatica-derived carbon dots. Carbon Lett. 2023. https://doi.org/10.1007/s42823-023-00505-3.
29. Navaneethan RD, et al. Green synthesis of luminescent carbon dots from ficus benghalensis aerial roots for bioimaging. J Fluoresc. 2024. https://doi.org/10.1007/s10895-024-03964-7.
30. De Lima Oliveira EG, et al. Green synthesis of fluorescent carbon dots/silver nanoparticles with enhanced antibacterial activity. Braz J Chem Eng. 2024. https://doi.org/10.1007/s43153-024-00512-5.
31. Parveen S, et al. Green synthesis of value-added fluorescent carbon dots from sugarcane bagasse and their antioxidant, reducing and catalytic activities. Sugar Tech. 2024. https://doi.org/10.1007/s12355-023-01317-5.
32. Nasseri MA, et al. Phytochemical properties and antioxidant activity of Echinops persicus plant extract: green synthesis of carbon quantum dots from the plant extract. SN Appl Sci. 2020. https://doi.org/10.1007/s42452-020-2466-0.
33. Hak CH, et al. Water hyacinth derived carbon quantum dots and g-C3N4 composites for sunlight driven photodegradation of 2,4-dichlorophenol. SN Appl Sci. 2020. https://doi.org/10.1007/s42452-020-2840-y.
34. Petruzzello, M. (2024). amaranth. *Encyclopaedia Britannica*.
35. Yudhistira B, et al. Effect of green spinach (*Amaranthus* tricolor L.) and tomato (*Solanum lycopersicum*) addition in physical, chemical, and sensory properties of marshmallow as an alternative prevention of iron deficiency anemia. IOP Conf Ser: Earth Environ Sci. 2018. https://doi.org/10.1088/1755-1315/102/1/012007.
36. Minal Belekar*, S.B. Exploring The Phytochemical and Pharmacological Review on *Amaranthus* Tricolor. (2024). https://doi.org/10.5281/ZENODO.14310395
37. Spórna-Kucab A, et al. Antioxidant and antimicrobial effects of baby leaves of *Amaranthus* tricolor L. Harvested as vegetable in correlation with their phytochemical composition. Molecules. 2023. https://doi.org/10.3390/molecules28031463.
38. Baraniak J, Kania-Dobrowolska M. The dual nature of amaranth—functional food and potential medicine. 2022. Foods. https://doi.org/10.3390/foods11040618.

39. Akter MR, et al. Comparative assessment of free radical scavenging, membrane stabilizing and thrombolytic potentials of two *Amaranthus* species of Bangladesh. Bangladesh J Bot. 2022;51:139.
40. D'Amico, S. and Schoenlechner, R. Chapter 6 - Amaranth: Its Unique Nutritional and Health-Promoting Attributes, in *Gluten-Free Ancient Grains* (eds.Taylor, J.R.N. and Awika, J.M.), Woodhead Publishing, (2017). pp. 131–159.
41. Sreelathakumary, I. and Peter, K.V. 22 - Amaranth: Amarathus spp., in *Genetic Improvement of Vegetable Crops* (eds.Kalloo, G. and Bergh, B.O.), Pergamon, Amsterdam, (1993). pp. 315–323.
42. Sattar M, et al. An overview of the nutritional and therapeutic properties of amaranth. Int J Food Prop. 2024. https://doi.org/10.1080/10942912.2024.2304266.
43. Waheed SM, et al. Deep vein thrombosis, in *StatPearls*. Treasure Island (FL): StatPearls Publishing; 2025.
44. Manoharan RR, et al. ROS signaling in innate immunity via oxidative protein modifications. Front Immunol. 2024. https://doi.org/10.3389/fimmu.2024.1359600.
45. Kong AS-Y, et al. Oxidative stress parameters as biomarkers of cardiovascular disease towards the development and progression. Antioxidants. 2022. https://doi.org/10.3390/antiox11061175.
46. Vallelian F, et al. Hemolysis, free hemoglobin toxicity, and scavenger protein therapeutics. Blood. 2022. https://doi.org/10.1182/blood.2022015596.
47. Valaitienė J, Laučytė-Cibulskienė A. Oxidative stress and its biomarkers in cardiovascular diseases. Artery Res. 2024. https://doi.org/10.1007/s44200-024-00062-8.
48. https://www.osmosis.org/answers/coagulation-cascade.
49. Litvinov RI, Weisel JW. Blood clot contraction: mechanisms, pathophysiology, and disease. Res Pract Thromb Haemost. 2023. https://doi.org/10.1016/j.rpth.2022.100023.
50. Chahardoli A, et al. Optimization of quercetin-assisted silver nanoparticles synthesis and evaluation of their hemocompatibility, antioxidant, anti-inflammatory, and antibacterial effects. Global Chall. 2021. https://doi.org/10.1002/gch2.202100075.
51. Watcharamongkol T, et al. Green hydrothermal synthesis of multifunctional carbon dots from cassava pulps for metal sensing, antioxidant, and mercury detoxification in plants. Carb Res Convers. 2024. https://doi.org/10.1016/j.crcon.2023.100206.
52. Han B, et al. Synthesis of carbon dots with hemostatic effects using traditional Chinese medicine as a biomass carbon source. ACS Omega. 2023. https://doi.org/10.1021/acsomega.2c06600.
53. Singh SR, et al. The effect of *Clitoria ternatea* L flowers-derived silver nanoparticles on A549 and L-132 human cell lines and their antibacterial efficacy in *Caenorhabditis* elegans in vivo. Hybrid Adv. 2025. https://doi.org/10.1016/j.hybadv.2024.100359.
54. Pujar R, et al. GC-MS based phytochemical profiling and investigation of in vitro pharmacological activity of Croton sparsiflorus. Res J Biotechnol. 2022;17:8.
55. Sembiring EN, et al. Phytochemical screening, total flavonoid and total phenolic content and antioxidant activity of different parts of *Caesalpinia* bonduc (L.) Roxb. Pharmacogn J. 2017;10:123.
56. Institute of Medical Research and Medicinal Plants Studies, P.O. Box 6163, Yaoundé, Cameroon et al. Folin-Ciocalteau Reagent for Polyphenolic Assay. International Journal of Food Science, Nutrition and Dietetics. (2014). https://doi.org/10.19070/2326-3350-1400028
57. Bhatti MZ, et al. Antioxidant and phytochemical analysis of *Ranunculus arvensis* L. extracts. BMC Res Notes. 2015. https://doi.org/10.1186/s13104-015-1228-3.
58. Silva F, et al. A rapid and simplified DPPH assay for analysis of antioxidant interactions in binary combinations. Microchem J. 2024. https://doi.org/10.1016/j.microc.2024.110801.
59. Yang JY, et al. Analysis and phytochemical profile of *Amaranthus* tricolor L. extract with antioxidative and antimicrobial properties. Food Sci Technol. 2023. https://doi.org/10.5327/fst.004823.
60. Bhat S, Rajanna L. Preliminary phytochemical analysis and in vitro antioxidant potential of fruit stalk of capsicum annuum var. *glabriusculum* (Dunal) Heiser & Pickersgill. J Pharm Sci. 2017;9:1283.
61. Sun W, Shahrajabian MH. Therapeutic potential of phenolic compounds in medicinal plants—natural health products for human health. Molecules. 2023. https://doi.org/10.3390/molecules28041845.
62. Dugam S, et al. Carbon dots: a novel trend in pharmaceutical applications. Ann Pharm Fr. 2021. https://doi.org/10.1016/j.pharma.2020.12.002.
63. Manzoor S, et al. Carbon dots applications for development of sustainable technologies for food safety: a comprehensive review. Appl Food Res. 2023. https://doi.org/10.1016/j.afres.2023.100263.
64. Tejwan N, et al. Synthesis of green carbon dots as bioimaging agent and drug delivery system for enhanced antioxidant and antibacterial efficacy. Inorg Chem Commun. 2022. https://doi.org/10.1016/j.inoche.2022.109317.
65. Masyita A, et al. Terpenes and terpenoids as main bioactive compounds of essential oils, their roles in human health and potential application as natural food preservatives. Food Chem: X. 2022. https://doi.org/10.1016/j.fochx.2022.100217.
66. Rai S, et al. Plant-derived saponins: a review of their surfactant properties and applications. Sci. 2021. https://doi.org/10.3390/sci3040044.
67. Martins JN, et al. Selective recognition of amino acids and peptides by small supramolecular receptors. Molecules. 2020. https://doi.org/10.3390/molecules26010106.
68. Lozano-Grande MA, et al. Plant sources, extraction methods, and uses of squalene. Int J Agron. 2018. https://doi.org/10.1155/2018/1829160.
69. Balachandran, A. et al. Antioxidant, Wound Healing Potential and In Silico Assessment of Naringin Eicosane and Octacosane. *Molecules*. (2023). https://doi.org/10.3390/molecules28031043.
70. Pradhan S, Dubey RC. Molecular docking of a bioactive compound of C. sinensis n-heptadecanol-1 with opportunistic fungi. Curr Res Gr Sustain Chem. 2021. https://doi.org/10.1016/j.crgsc.2021.100208.
71. Althagafi I. Molecular modeling and antioxidant evaluation of new di-2-thienyl ketones festooned with thiazole or pyridine moiety. J Mol Struct. 2022. https://doi.org/10.1016/j.molstruc.2021.131287.
72. Api AM, et al. RIFM fragrance ingredient safety assessment, 2-heptyltetrahydrofuran, CAS Registry Number 2435–16-7. Food Chem Toxicol. 2024. https://doi.org/10.1016/j.fct.2023.114374.

73. Lee S-H, et al. Identification of plant compounds that disrupt the insect juvenile hormone receptor complex. Proc Natl Acad Sci. 2015. https://doi.org/10.1073/pnas.1424386112.
74. Ozyurt D, et al. Properties, synthesis, and applications of carbon dots: a review. Carbon Trends. 2023. https://doi.org/10.1016/j.cartre.2023.100276.
75. Mmelesi OK, et al. Recent development in fluorescent carbon quantum dots-based photocatalysts for water and energy applications. Mater Sci Semicond Process. 2024. https://doi.org/10.1016/j.mssp.2024.108661.
76. Saputra AMA, et al. Synthesis, properties, and utilization of carbon quantum dots as photocatalysts on degradation of organic dyes: a mini review. Catal Commun. 2024. https://doi.org/10.1016/j.catcom.2024.106914.
77. Bhavi SM, et al. Biogenic silver nanoparticles from *Simarouba glauca* DC leaf extract: synthesis, characterization, and anticancer efficacy in lung cancer cells with protective effects in *Caenorhabditis* elegans. Nano TransMed. 2024. https://doi.org/10.1016/j.ntm.2024.100052.
78. Zhang C, et al. Thermal stability of CsPbBr 3 perovskite as revealed by *in sit*u transmission electron microscopy. APL Mater. 2019. https://doi.org/10.1063/1.5108849.
79. Wang F, et al. Application of carbon quantum dots as fluorescent probes in the detection of antibiotics and heavy metals. Food Chem. 2025. https://doi.org/10.1016/j.foodchem.2024.141122.
80. Siddeeg A, et al. Mode of action and determination of antioxidant activity in the dietary sources: an overview. Saudi J Biol Sci. 2021. https://doi.org/10.1016/j.sjbs.2020.11.064.
81. Rodríguez-Varillas S, et al. Biocompatibility and antioxidant capabilities of carbon dots obtained from tomato (*Solanum lycopersicum*). Appl Sci. 2022. https://doi.org/10.3390/app12020773.
82. Li P, et al. Understanding thrombosis: the critical role of oxidative stress. Hematology. 2024. https://doi.org/10.1080/16078454.2023.2301633.
83. Nwankwo NE, et al. Bioactive compounds, anti-inflammatory, anti-nociceptive and antioxidant potentials of ethanolic leaf fraction of Sida linifolia L. (*Malvaceae*). Arab J Chem. 2023. https://doi.org/10.1016/j.arabjc.2022.104398.
84. Chahardoli A, et al. Galbanic acid, a sesquiterpene coumarin as a novel candidate for the biosynthesis of silver nanoparticles: In vitro hemocompatibility, antiproliferative, antibacterial, antioxidant, and anti-inflammatory properties. Adv Powder Technol. 2023. https://doi.org/10.1016/j.apt.2022.103928.
85. Chahardoli A, et al. Isoimperatorin-mediated green-synthesized silver nanoparticles: antibacterial, antioxidant, cytotoxicity, hemolytic and coagulation effects. Bull Mater Sci. 2022. https://doi.org/10.1007/s12034-022-02665-w.
86. Chahrdoli A, et al. Achillea wilhelmsii C. Koch mediated blood compatible silver nanoparticles. Mater Today Commun. 2020. https://doi.org/10.1016/j.mtcomm.2020.101577.
87. González-Martínez GA, et al. Hydrothermal synthesis of carbon quantum dots from Citrus limetta peels: exploration of pH sensing, non-hemolytic activity and thermoluminescent properties. Mater Lett. 2024. https://doi.org/10.1016/j.matlet.2024.137119.

Publisher's Note Springer Nature remains neutral with regard to jurisdictional claims in published maps and institutional affiliations.